Clim Dyn (2012) 39:1951–1968
DOI 10.1007/s00382-012-1300-9

Global response to solar radiation absorbed by phytoplankton in a coupled climate model

Lavinia Patara · Marcello Vichi · Simona Masina · Pier Giuseppe Fogli · Elisa Manzini

Received: 29 June 2011 / Accepted: 16 January 2012 / Published online: 11 February 2012

Abstract The global climate response to solar radiation absorbed by phytoplankton is investigated by performing multi-century simulations with a coupled ocean–atmosphere-biogeochemistry model. The absorption of solar radiation by phytoplankton increases radiative heating in the near-surface ocean and raises sea surface temperature (SST) by overall $\sim$0.5°C. The resulting increase in evaporation enhances specific atmospheric humidity by 2–5%, thereby increasing the Earth's greenhouse effect and the atmospheric temperatures. The Hadley Cell exhibits a weakening and poleward expansion, therefore reducing cloudiness at subtropical-middle latitudes and increasing it at tropical latitudes except near the Equator. Higher SST at polar latitudes reduces sea ice cover and albedo, thereby increasing the high-latitude ocean absorption of solar radiation. Changes in the atmospheric baroclinicity cause a poleward intensification of mid-latitude westerly winds in both hemispheres. As a result, the North Atlantic Ocean meridional overturning circulation extends more northward, and the equatorward Ekman transport is enhanced in the Southern Ocean. The combination of local and dynamical processes decreases upper-ocean heat content in the Tropics and in the subpolar Southern Ocean, and increases it at middle latitudes. This study highlights the relevance of coupled ocean–atmosphere processes in the global climate response to phytoplankton solar absorption. Given that simulated impacts of phytoplankton on physical climate are within the range of natural climate variability, this study suggests the importance of phytoplankton as an internal constituent of the Earth's climate and its potential role in participating in its long-term climate adjustments.

Keywords Coupled climate model · Bio-physical interactions · Solar radiation · Climate · Marine biogeochemical model · Phytoplankton radiative heating · Ocean circulation

L. Patara (✉) · M. Vichi · S. Masina · P. G. Fogli · E. Manzini
Centro Euro-Mediterraneo per i Cambiamenti Climatici (CMCC), Viale Aldo Moro 44, 40127 Bologna, Italy
e-mail: lpatara@geomar.de

Present Address:
L. Patara
Helmholtz Centre for Ocean Research Kiel (GEOMAR), Düsternbrooker Weg 20, 24105 Kiel, Germany

M. Vichi · S. Masina
Centro Euro-Mediterraneo per i Cambiamenti Climatici (CMCC), Istituto Nazionale di Geofisica e Vulcanologia (INGV), Viale Aldo Moro 44, 40127 Bologna, Italy

Present Address:
E. Manzini
Max-Planck-Institut für Meteorologie, Hamburg, Germany

1 Introduction

Marine biogeochemistry is a relevant player within the Earth System. Marine biogeochemical properties are in fact largely determined by the physical environment, yet they are themselves capable of modifying the physical climate through exchanges of mass and energy. It is suggested that a potentially relevant biological effect on the global climate may arise from the interaction between the ocean's bio-optical state and the vertical profiles of solar radiation in the upper ocean (Morel and Antoine 1994). Phytoplankton organisms, which dwell in the upper 100 m of the ocean, strongly absorb shortwave radiation for photosynthesis. Since solar radiation absorption leads to ocean radiative heating, the presence of phytoplankton gives rise to an increase in radiative heating in the near-surface

Table 1 A selection of representative studies on the effects of phytoplankton heating using different model designs (*OGCM* ocean general circulation model; *CGCM* coupled general circulation model) and different attenuation depths for visible radiation in the control experiment. These studies investigate the phytoplankton effects on sea surface temperature (SST) in the Tropical Pacific, in the extratropical Northern Hemisphere, and in the Southern Ocean (the SST changes have been extracted visually from the cited literature and are thus approximate). "Prescribed chlorophyll" indicates the use of satellite ocean colour to estimate biological attenuation depths, whereas "interactive marine biogeochemistry" indicates the coupling with a marine biogeochemistry model

	Model design	Attenuation depth in the control simulation (m)	Feedback on Tropical Pacific SST (°C)	Feedback on Northern Hemisphere SST (°C)	Feedback on Southern Ocean SST (°C)
Murtugudde et al. (2002)	OGCM, prescribed chlorophyll	17	+1 to +2	×	×
Oschlies (2004)	OGCM, interactive marine biogeochemistry	25	×	+0.5	×
Manizza et al. (2005)	OGCM, interactive marine biogeochemistry	23	−0.3	+0.2	+0.5
Löptien et al. (2009)	Eddy permitting OGCM, interactive marine biogeochemistry	23	−1	×	×
Wetzel et al. (2006)	CGCM, interactive marine biogeochemistry	11	+0.5	+0.5	<|0.2|
Lengaigne et al. (2007, 2009)	CGCM, interactive marine biogeochemistry	~23	+0.5	+0.5 to +1	×
Gnanadesikan and Anderson (2009)	CGCM, prescribed chlorophyll	43	−1 to −2	+1 to +2	−1
This study	CGCM, interactive marine biogeochemistry	23	+0.2 to +0.5	+0.5 to +1	+0.5

ocean. The potential relevance of biological radiative heating within the Earth's climate is related to some key characteristics of phytoplankton at the global scale. Phytoplankton organisms are in fact (1) at the base of marine ecosystems and virtually ubiquitous in the global ocean, (2) they dwell in the upper-ocean layers where the coupling with the atmosphere is strongest, and (3) their abundance and temporal evolution are tightly linked with the Earth's physical climate. A new question is if phytoplankton radiative heating may have a role in affecting the Earth's climate and its adjustment to internal and external climate variations.

This question is particularly urgent in today's climate science, as most climate models used to predict climate impacts of anthropogenic CO_2 emissions do not contain an interactive marine biogeochemistry model (Meehl et al. 2007). Instead, many use a constant attenuation depth for visible radiation of ~20 m depth, typical of open ocean conditions (Jerlov 1968; Paulson and Simpson 1977). This parameterization however does not consider the large variations of bio-optical properties and associated radiative heating that can be found throughout the ocean on various temporal and spatial scales (Sathyendranath et al. 1991; Strutton and Chavez 2004). Unfortunately, the observational quantification of the effects of phytoplankton radiative heating onto physical climate properties is made difficult by the fact that phytoplankton organisms are always present in the Earth System, and a "control" situation without phytoplankton does not exist. Consequently, modeling frameworks have been used to investigate several aspects of the climate response to phytoplankton radiative heating.

The model designs employed in previous studies range from ocean and atmosphere general circulation models to fully coupled ocean–atmosphere general circulation models (hereafter CGCM), and from prescribed to interactive marine biogeochemistry (a selection of the literature is shown in Table 1). A region in which impacts of biological radiative heating have been extensively studied is the Tropical Pacific. Here elevated phytoplankton concentrations, combined with a strong ocean–atmosphere coupling, are thought to influence the mean climate state (Schneider and Zhu 1998; Shell et al. 2003; Sweeney et al. 2005; Lengaigne et al. 2007; Gnanadesikan and Anderson 2009; Gnanadesikan et al. 2010), its variability (Timmermann and Jin 2002; Marzeion et al. 2005; Anderson et al. 2009; Jochum et al. 2010), and the activity of tropical cyclones (Gnanadesikan et al. 2010). However, in spite of the numerous studies, it is still uncertain whether the presence of phytoplankton increases or decreases tropical Pacific sea surface temperature (Table 1). For instance, Murtugudde et al. (2002) and Marzeion et al. (2005) detected a surface warming of up to 2°C associated with a deepening of the mixed layer depth (hereafter MLD). Other authors found

instead that phytoplankton leads to a surface cooling of $\sim$1°C associated with shoaling of the equatorial MLD and enhancement of the Southern Equatorial Current (Nakamoto et al. 2001), or with a reduction of the integrated equatorward ocean heat transport (Sweeney et al. 2005; Manizza et al. 2008; Löptien et al. 2009). Anderson et al. (2007) and Gnanadesikan and Anderson (2009) detected an equatorial sea surface temperature (hereafter SST) decrease caused by changes in off-equatorial ocean water clarity: in fact when ocean color is present, the equatorward branch of the shallow meridional overturning cells transports cooler waters than when ocean color is absent.

The ocean–atmosphere coupling adds further complexity to the phytoplankton impact on the Tropical Pacific climate. In their early CGCM study, Schneider and Zhu (1998) already suggested that changing the penetration of solar radiation in the tropical Pacific could affect the SST sensitivity to upwelling, and that this would have an effect on maintaining the tropical atmospheric convection closer to the Equator. Lengaigne et al. (2007) found in their CGCM study that biologically-induced surface warming (up to 0.5°C) in the eastern Tropical Pacific causes a $\sim$10% weakening of easterly trade winds: this would provide a positive feedback on SST by weakening ocean upwelling. Wetzel et al. (2006) detected an intensification of the Hadley Cell in response to a phytoplankton-induced increase in equatorial SST. In their atmosphere general circulation model (hereafter AGCM) Shell et al. (2003) described a similar impact on the Hadley Cell, even though the response was of opposite sign since their AGCM was forced by a reduction of equatorial SST.

Phytoplankton radiative heating was suggested to exert climate effects also at extratropical latitudes. Oschlies (2004), Manizza et al. (2008) and Gnanadesikan and Anderson (2009) found that the presence of phytoplankton enhances the seasonal cycle of mid-latitude SST and ocean mixing. In fact, increased radiation absorption in the surface ocean causes subsurface radiative cooling which is entrained to the surface during winter. In their CGCM study, Lengaigne et al. (2009) found that the presence of phytoplankton increases Arctic SST, precipitation and runoff, thereby reducing Arctic sea ice volume by 17%. In their model, the combination of these effects is responsible for a $\sim$15% reduction of the North Atlantic meridional overturning circulation. In the Southern Ocean, Gnanadesikan and Anderson (2009) found that the influence of phytoplankton on extratropical SST and on wind stress curl causes a reduction of the southern hemisphere meridional overturning circulation and of the formation of subtropical mode water.

Past research clearly shows that the overall impact of phytoplankton on the climate system depends on whether oceanic and atmospheric processes amplify or damp the phytoplankton local heating. Yet these studies show strikingly different responses of SST to biological radiative heating. This diversity may be due to (1) the large spread of modeling strategies, concerning both the physical climate components and the presence or not of interactive marine biogeochemistry (Table 1), (2) the different ways in which radiation is treated in the control experiments (Table 1), and (3) the simulation length and whether it is still adjusting to phytoplankton radiative heating. As a result, assessing the robustness of the climate responses to phytoplankton and disentangling the relative importance of different processes is still a difficult task.

The aim of this study is to further assess the phytoplankton influences on global climate by exploiting a state-of-the-art coupled climate model containing interactive marine biogeochemistry. Two 300-year simulations are performed, one using a constant attenuation depth of 23 m typical of clear open-ocean waters (Jerlov 1968), the other having an additional attenuation term for solar radiation due to the time- and space- varying marine biogeochemistry. This experimental design is useful for a number of reasons: (1) the modeled physical climate and marine biogeochemistry vary temporally and spatially in a coherent manner, (2) these experiments may easily be compared with other CGCM simulations, which typically use constant attenuation depths of 23 m, and (3) the multi-centennial scale simulations allows for an analysis of the phytoplankton effects once the physical climate has adjusted to the presence of phytoplankton. This experimental design resembles that used by Wetzel et al. (2006) and Lengaigne et al. (2007, 2009), whose simulations however were around 100 years long, thus shorter than the simulations carried out for this study. The objectives of this study are (1) to identify the processes through which phytoplankton radiative heating affects physical climate properties, (2) to quantify the climatic relevance of these processes, and (3) to estimate whether these processes enhance or damp the near-surface heating due to phytoplankton.

This article is organized as follows. Section 2 describes the coupled model components, the experimental design, as well as the treatment of solar radiation penetration in the ocean model. Section 3 shows the results of this work: Sect. 3.1 focuses on the comparison of the simulated climatologies with observed data sets, Sect. 3.2 shows how phytoplankton modifies ocean radiative heating, Sect. 3.3 shows how ocean and atmospheric temperatures are affected by phytoplankton through changes in surface heat fluxes and albedo, Sect. 3.4 investigates how changes in atmospheric temperatures modify the atmospheric circulation, and how this in turn affects the oceanic circulation and heat transport, and Sect. 3.5 provides a synthesis of the

results by quantifying the changes of ocean radiative and advective heating due to the presence of phytoplankton. Finally, Sect. 4 summarizes and discusses the main findings of this study.

2 Methods

2.1 Model description

The employed CGCM (Fogli et al. 2009) has been used in previous studies of North Atlantic oceanic and biogeochemical variability (Patara et al. 2011), of oceanic carbon uptake under anthropogenic carbon emission scenarios (Vichi et al. 2011), and in the ENSEMBLES multi-model experiments to deduce climate change under an aggressive mitigation scenario (Johns et al. 2011).

The ocean general circulation model OPA8.2 (Madec et al. 1998) is implemented on the global curvilinear and tripolar ORCA2 grid (Madec and Imbard 1996) having a horizontal resolution of $2°\times2°\ \cos\theta$ except for enhanced resolution (up to $0.5°\times0.5°$) in the 20°S–20°N tropical belt. In the vertical a z-coordinate is used with a total of 31 unevenly spaced vertical levels having enhanced resolution in the upper ocean. Vertical eddy diffusion of momentum and tracers is parameterized according to a 1.5 turbulent closure model based on a prognostic equation for the turbulent kinetic energy (Blanke and Delecluse 1993). The horizontal diffusion of momentum is parameterized with a Laplacian operator and the horizontal diffusion of tracers is computed by means of a harmonic operator along isopycnal surfaces with an eddy diffusivity coefficient equal to 2,000 $m^2\ s^{-1}$. The model implements an eddy-induced velocity parameterization (Gent and McWilliams 1990) with coefficient values usually varying between 15 and 3,000 $m^2\ s^{-1}$. The ocean model includes the LIM2 dynamics and thermodynamics sea ice model (Timmermann et al. 2005) which includes the sensible heat storage and vertical heat conduction within snow and ice by means of a three-layer model (one layer for snow and two layers for ice).

The atmosphere general circulation model is ECHAM5 (Röckner et al. 2003), which numerically solves the primitive equations on a sphere by means of the spectral transform method. The horizontal triangular truncation used is T31, corresponding to an approximate 3.75° horizontal grid spacing. In the vertical a hybrid coordinate is used with a total of 19 unevenly spaced vertical levels and top at 10 hPa. The ocean and atmosphere exchange momentum, heat, and freshwater fluxes once a day by means of the OASIS3 coupler (Valcke et al. 2004; Fogli et al. 2009) which ensures heat and freshwater conservation without the addition of flux corrections. Since river runoff is climatologically prescribed, excess or deficit of freshwater is equally redistributed on the global ocean on a daily basis.

The marine biogeochemistry model PELAGOS (Vichi et al. 2007a) is the global ocean implementation of the Biogeochemical Flux Model (BFM, http://bfm.cmcc.it) and has shown skill at reproducing observed climatologies and interannual variability of biogeochemical properties (Vichi et al. 2007b; Vichi and Masina 2009; Patara et al. 2011). The model includes a comprehensive set of marine biogeochemistry relations for major inorganic and organic compounds and for the lower trophic levels of the marine ecosystem. Three phytoplankton groups (diatoms, nano- and picophytoplankton), three zooplankton groups (nano-, micro-, and mesozooplankton), and one bacterioplankton group are described according to their physiological requirements and feeding interactions. Nutrient uptake is parameterized following a Droop kinetics (Vichi et al. 2007a) which allows for multi-nutrient limitation and variable internally-regulated nutrient ratios. Chlorophyll synthesis is down-regulated when the rate of light absorption exceeds the utilization of photons for carbon fixation (Geider et al. 1997). Dissolved inorganic iron is explicitly simulated and treated as an internal constituent of phytoplankton (Vichi et al. 2007a).

2.2 Experiment set up

The CGCM is used to produce two simulations: experiment A (standing for Abiotic) is performed only with the physical components of the coupled model described in Sect. 2.1. The simulation is initialized using World Ocean Atlas 1998 climatologies for ocean temperature and salinity (Levitus et al. 1998) and is integrated for 400 years. Experiment B (standing for Biotic) uses the same physical model as experiment A with the addition of the marine biogeochemistry model PELAGOS. Experiment B is initialized with the year 100 of experiment A for the physics and is integrated for 300 years. World Ocean Atlas 2001 climatologies (Conkright et al. 2002) are used to initialize macronutrients, GLODAP climatologies (Key et al. 2004) are used to initialize dissolved inorganic carbon and alkalinity, and uniform concentrations are prescribed for the remaining variables. Both simulations are integrated using constant atmospheric CO_2 concentrations of 348 ppm, and Fortuin and Kelder (1998) ozone concentration climatologies. These are approximate present climate conditions for well-mixed greenhouse gases and ozone.

2.3 Solar radiation in the ocean

In the ocean model, downwelling solar radiation is partitioned as 42% shortwave (or visible) and 58% longwave

(or infrared), and is exponentially absorbed within the water column with an e-folding depth (or attenuation depth) of 0.01 m for infrared radiation and of 23 m for visible radiation. These values derive from observational fits in open ocean conditions reported by Jerlov (1968) and Paulson and Simpson (1977). Whereas infrared radiation is totally absorbed in the first ocean model layer, visible radiation may reach $\sim$100 m depth. When phytoplankton is present, the attenuation of visible radiation additionally depends on the depth-dependent diffuse attenuation coefficient $k_{bio}(z)$ which is treated as a linear function of chlorophyll content and, to a lesser extent, of detrital matter (Vichi et al. 2007a). The attenuation coefficient for visible radiation $k_{VIS}(z)$, i.e. the inverse of the attenuation depth, is computed at each depth z as:

$$k_{VIS}(z) = k_w + \frac{1}{z}\int_z^0 k_{bio}(z')dz', \qquad (1)$$

where k_w is the constant visible attenuation coefficient for seawater ($1/k_w = 23$ m). The B experiment (containing biogeochemistry) is thus generally characterized by shallower attenuation depths than the A experiment, especially where chlorophyll values are highest (as it will be shown in Sect. 3.2).

In the ocean model, solar radiation absorption causes radiative heating according to:

$$\frac{\partial T}{\partial t} = \frac{1}{\rho\, C_P}\frac{\partial I}{\partial z}, \qquad (2)$$

where I is the solar radiation incident at the ocean surface, C_p is the specific ocean heat capacity (set uniformly to 4,000 J K^{-1} kg^{-1}), and ρ is ocean density.

3 Results

3.1 Simulated climatologies and comparison with observations

Figure 1 shows simulated annual climatologies of SST (Fig. 1a, contours) and wind stress (Fig. 1b, arrows) over the last 150 years of the A experiment, and their biases (colors) with respect to the Hadley SST data set (Rayner et al. 2003) and the ERA-40 reanalysis (Uppala et al. 2005). SST is underestimated by $\sim$2°C in the equatorial Pacific cold tongue and by $\sim$6°C in the North Atlantic subpolar ocean, whereas it is overestimated by $\sim$6°C in the eastern boundaries of tropical oceans and in the North Pacific mid-latitudes. These SST biases are known to affect, with similar magnitudes, most climate models used for the IPCC-AR4 Report (Fig. 8.2 of Randall et al. 2007). Easterly trade winds and mid-latitude westerly winds are overall

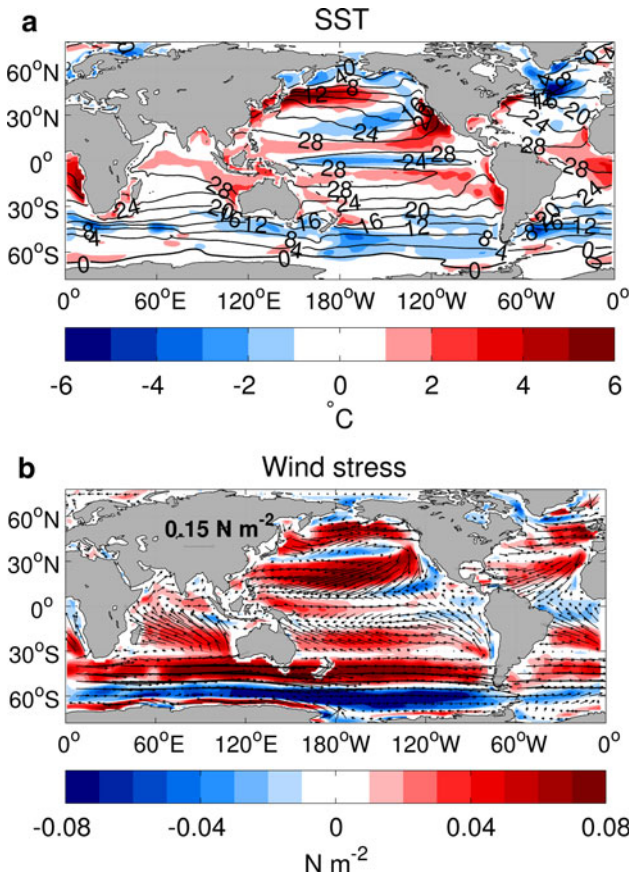

Fig. 1 *Experiment A* annual climatologies and biases: **a** sea surface temperature (SST) in °C (*contours*) and bias with respect to Hadley SST (*colors*), **b** wind stress in N m^{-2} (*arrows*) and bias with respect to ERA-40 reanalysis (*colors*)

overestimated over the North Atlantic and North Pacific Oceans by $\sim$0.1 N m^{-2} (Fig. 1b, colors). Westerly winds over the Southern Ocean are shifted equatorward, as also detected in a number of pre-industrial climate model simulations used for the IPCC-AR4 report (Russell et al. 2006).

Figure 2a shows annual chlorophyll concentrations in the B experiment averaged over the euphotic layer, i.e. the depth at which sunlight is 1% of the incident solar radiation at the ocean surface. Simulated chlorophyll values are compared with satellite SeaWiFS estimates (McClain 2009) averaged over the years 1998–2006 (Fig. 2b). The model captures the main spatial features of the chlorophyll field, i.e. the maxima at subpolar and equatorial latitudes and the minima at subtropical latitudes. Also the chlorophyll depth structure compares well to observed World Ocean Atlas 2009 data (Garcia et al. 2010), as it can be seen in the zonally-averaged chlorophyll concentrations (Fig. 3, contours) characterized by a deep chlorophyll maximum at $\sim$80 m depth at tropical latitudes ($\sim$0.3 mg m^{-3}) and shallower maxima at subpolar latitudes (>0.5 mg m^{-3}). However, the model tends to underestimate chlorophyll

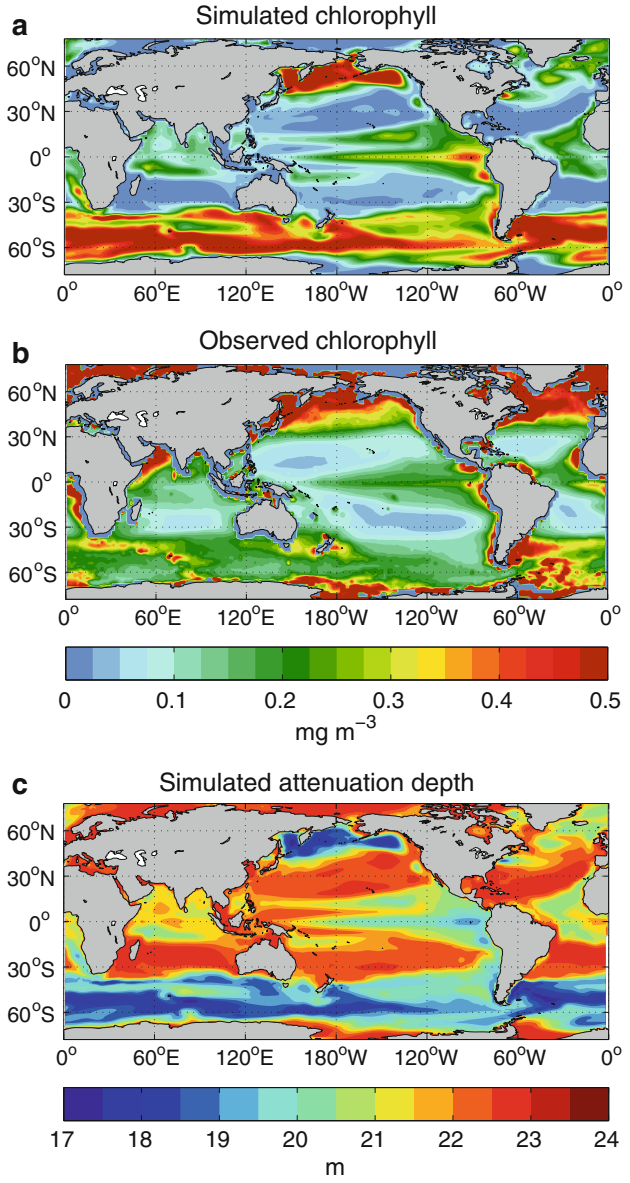

Fig. 2 Annual climatologies of **a** simulated chlorophyll concentration in the *B experiment* averaged over the euphotic layer (mg m^{-3}), **b** satellite SeaWiFS chlorophyll concentration (mg m^{-3}) averaged over the years 1998–2006, **c** simulated attenuation depths for visible radiation (m) in the *B experiment*

concentration in the Subtropics and in the North Atlantic and to overestimate it in the Southern Ocean. In the North Atlantic, the underestimation is possibly caused by an unbalance between export of organic matter into deep ocean layers and nutrient re-supply into the euphotic layer, whereas in the subtropical gyres the chlorophyll underestimation is caused by too shallow MLDs (Patara et al. 2011). In the Southern Ocean, stronger-than-observed MLD seasonal cycles at mid-latitudes conjure with abundant upwelled nutrients to produce the overestimated chlorophyll concentrations (Vichi and Masina 2009).

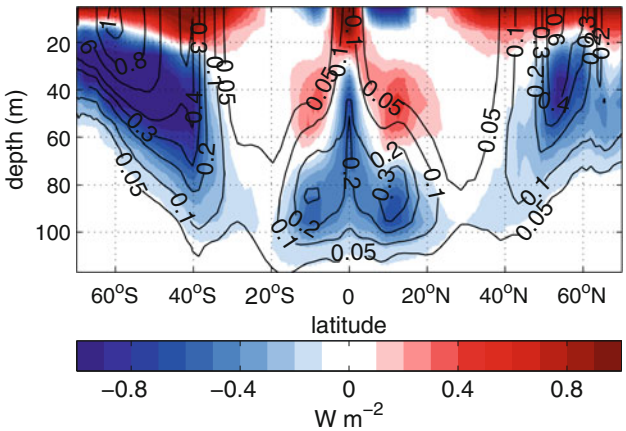

Fig. 3 *Contours*: zonal average of chlorophyll concentration (mg m^{-3}) in the *B experiment*, *colors*: zonal average of $B - A$ differences in radiative heating (W m^{-2})

3.2 Phytoplankton solar radiation absorption

In the areas where chlorophyll is highest, i.e. in the Tropics and at subpolar latitudes, the B experiment is characterized by shallower attenuation depths than the A experiment (Fig. 2c). Here, attenuation depths in the B experiment are <20 m, whereas in the subtropical gyres they are closer the attenuation depths in the A experiment (i.e. 23 m). The shallower attenuation depths in the B experiment cause a higher solar radiative heating in the upper ocean. This can be seen in Fig. 3 (colors) showing zonally-averaged differences in radiative heating between experiments B and A. Radiative heating differences (in W m^{-2}) are computed as the heating rate (K s^{-1}) multiplied by C_p, ρ and the model layer thickness. It can be seen that chlorophyll maxima are accompanied by positive $B - A$ differences of near-surface radiative heating (~ 1 W m^{-2}) and negative $B - A$ differences of subsurface radiative heating (-0.5 to -1 W m^{-2}). This is indicative of an upward shift of radiative heating profiles in the B with respect to the A experiment, due to the local phytoplankton near-surface heat trapping (as also found by Lengaigne et al. 2007). However, as it will be shown in Sect. 3.3, changes in incident solar radiation between the two experiments also play a role.

3.3 Thermal responses

3.3.1 Ocean

Figure 4a shows globally and annually averaged ocean heat content integrated between the surface and 300 m depth in experiments A and B. In the A experiment, upper-ocean heat content oscillates around a value of 146.5×10^8 J m^{-2} and exhibits large decadal and multi-decadal oscillations of $\sim 0.5 \times 10^8$ J m^{-2} amplitude. In the B experiment, upper-ocean heat content shows a gradual

increase throughout the first 150 years of simulation, and it tends to adjust itself in the last ~150 years to a value $\sim 1 \times 10^8$ J m^{-2} higher than the A experiment. The upper-ocean heat content in the B experiment thus takes more than 100 years to adjust to the presence of biogeochemistry. Since this study deals with the adjusted phase of the B experiment, the analysis of the mean differences between the two experiments is hereafter shown over the last 150 years of each experiment.

Figure 4b shows B − A differences in 0–300 m ocean heat content, where only 95% significant values (computed with a *t* test) are shown. For reference, the A experiment climatology is depicted as contours. Upper-ocean heat content in the B experiment is higher than in the A experiment by up to 5×10^8 J m^{-2} at subtropical and middle latitudes, whereas it is lower by $\sim 3 \times 10^8$ J m^{-2} in the Tropics and in some high-latitude areas. It can be argued that these results may be affected by the global multi-decadal decrease in upper-ocean heat content during the last 100 years of the A experiment (Fig. 4a). We thus remark that the results shown in Fig. 4b remain virtually unchanged when computing B − A differences on previous time periods of the A experiment (not shown).

Figure 4c shows 95% statistically-significant B − A differences in zonally-averaged ocean temperature. At middle latitudes, ocean temperatures in the B experiment are higher throughout the upper-ocean (up to 0.5°C in the northern hemisphere). However, at tropical latitudes B − A ocean temperature differences are slightly positive near the surface and are negative (~0.2°C on zonal average) in two off-equatorial lobes at ~100 m depth. The depth structure of the B − A ocean temperature differences in the Tropics bears strong resemblance with the B − A changes in radiative heating shown in Fig. 3 (colors). This suggests a leading role of phytoplankton solar absorption in generating upper-ocean temperature differences in the Tropics, as also found by Lengaigne et al. (2007). At extratropical latitudes the model results show that this is less the case, possibly because of deeper winter mixed layer depths which enhance the exchange between surface and sub-surface levels.

B − A SST differences are positive and statistically-significant at 95% throughout most of the global oceans (Fig. 4d). The largest SST increases in the B experiment (>0.5°C) occur in the North Atlantic and North Pacific Oceans at ~45°N, in the Barents Sea, and in some parts of the Southern Ocean. B − A SST differences of up to 0.4°C are also found in the eastern part of the Tropical Pacific. The correspondence between largest SST increases in the B experiment and highest chlorophyll concentrations (Fig. 2a) suggests a relevant role of the increased near-surface radiative heating due to phytoplankton (Fig. 3). As shown in Table 1, increased Tropical Pacific SST caused by phytoplankton was also found in a number of past studies (e.g. Murtugudde et al. 2002; Wetzel et al. 2006; Lengaigne et al. 2007) but not in others (e.g. Nakamoto

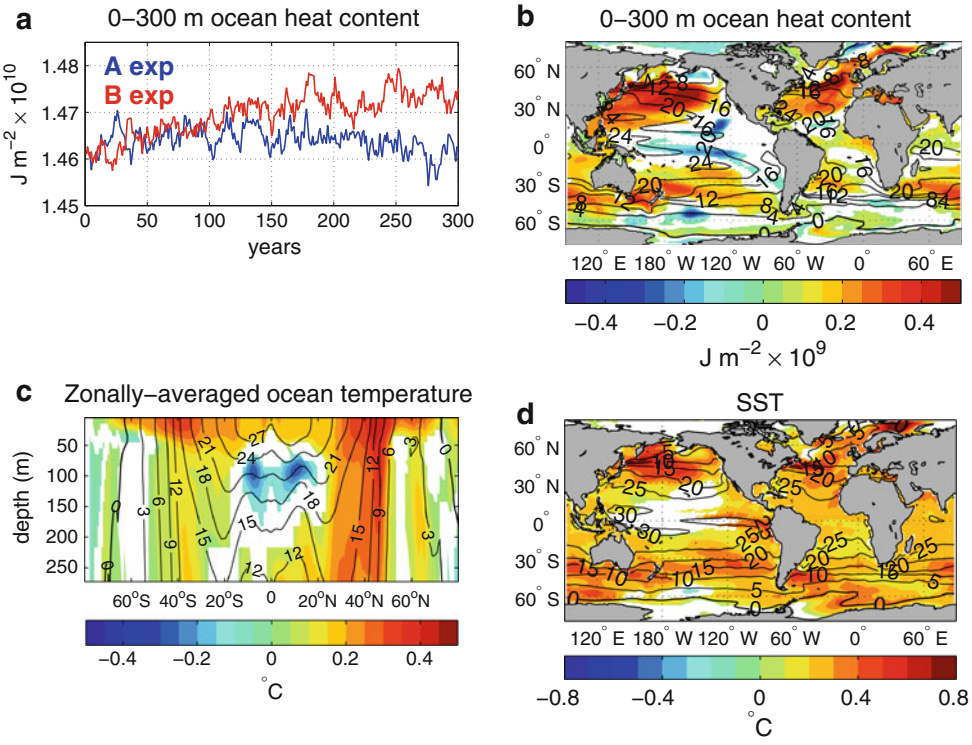

Fig. 4 **a** 300-year time series of globally and annually averaged ocean heat content integrated between 0 and 300 m depth (J m^{-2}) in the *A experiment* (*blue line*) and in the *B experiment* (*red line*), **b** *B* − *A* differences in ocean heat content integrated between 0 and 300 m depth (J m^{-2}) in *colors* and *A experiment* climatology in *contours* (spacing 4×10^9 J m^{-2}), **c** *B* − *A* differences in zonally-averaged ocean temperature (°C) in *colors* and *A experiment* climatology in *contours* (spacing 3°C), **d** *B* − *A* differences in sea surface temperature (SST) in °C and *A experiment* climatology in *contours* (spacing 5°C). **b–d** show only 95% statistically significant differences

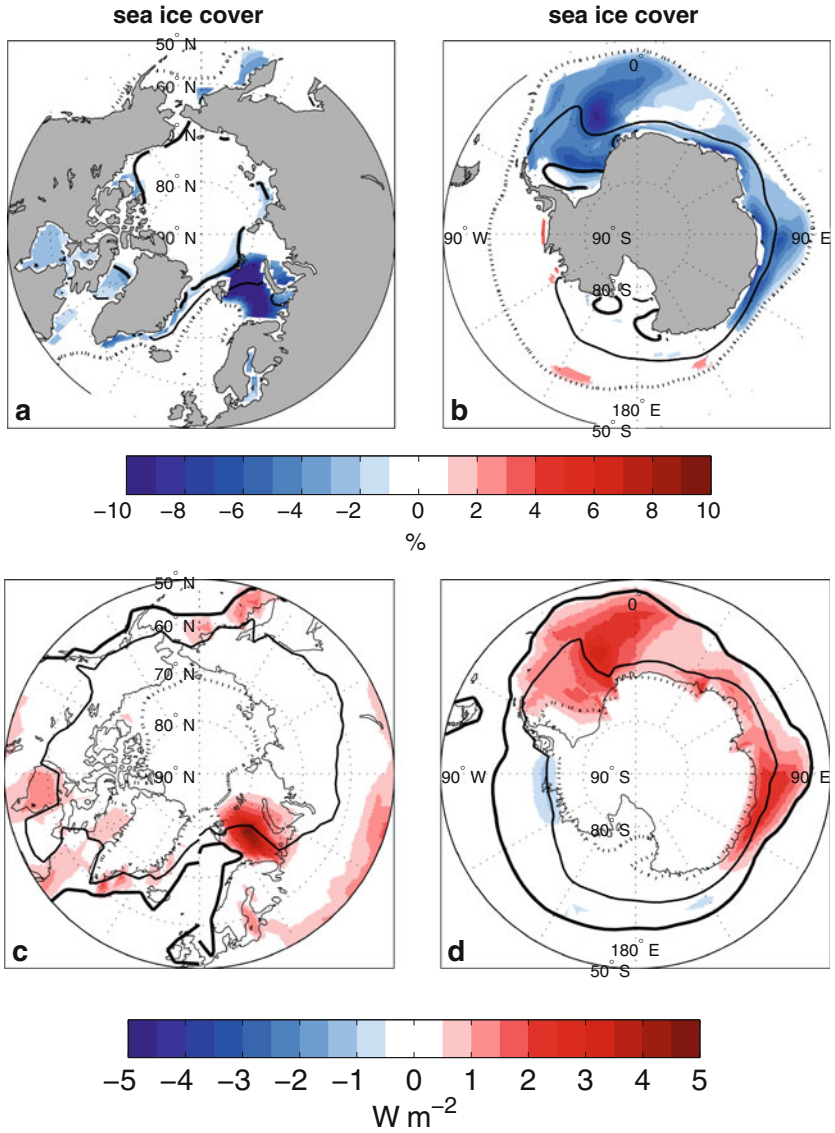

Fig. 5 *Top*: annual $B - A$ differences of sea ice cover (%) over **a** the northern hemisphere and **b** the southern hemisphere (*colors*); in *contours*, the 1% (*dashed line*), 50% (*full thin line*), and 90% (*full thick line*) sea ice cover in the *A experiment* are shown. *Bottom*: annual $B - A$ differences in albedo multiplied by incoming solar radiation in the *A experiment* (W m^{-2}) over **c** the northern hemisphere and **d** the southern hemisphere (*colors*); in *contours*, the 0.1 (*full thick line*), 0.4 (*full thin line*) and 0.7 (*dashed line*) albedo in the *A experiment* are shown. **a** and **b** show only 95% statistically-significant values

et al. 2001; Manizza et al. 2005; Gnanadesikan and Anderson 2009; Löptien et al. 2009). In the subpolar North Atlantic, increased summer SSTs due to phytoplankton near-surface heating were also found by Oschlies (2004) and Manizza et al. (2005, 2008), even though these authors also simulated lower winter SSTs due to the entrainment of cooler subsurface waters to the surface.

Annually-averaged sea ice cover is modified by up to 10% in the B with respect to the A experiment, in both the Arctic (Fig. 5a) and in the Antarctic (Fig. 5b). These changes are mostly occurring in the respective summer periods (not shown) and are a direct consequence of increased SST in the B with respect to the A experiment (Fig. 4d). In their CGCM study, Lengaigne et al. (2009) also detected an average decrease in Arctic sea ice cover of up to 10% during summer months, even though the largest sea ice decreases occurs in areas different than those found in this study (due to a different spatial pattern of the SST increases). In their OGCM study, Manizza et al. (2005) also detected a 10% annual decrease in Southern Ocean sea ice due to phytoplankton, in agreement with this study. However, contrarily to this study, in the Arctic Sea they found a slight increase in sea ice cover in all months except for the summer months.

Changes in sea ice cover induced by biology are capable of modifying the Earth's albedo, which is a measure of the Earth's reflectance. The multiplication between B and A differences in mean annual albedo and the incident solar radiation in the A experiment provides a measure of the changes in the radiation absorbed by the Earth's surface because of albedo changes. In the B experiment, the reduction in sea ice cover and albedo increases the surface absorption of solar radiation by up to 5 W m^{-2} in both the Arctic (Fig. 5c) and in the Antarctic (Fig. 5d). It can be expected that this will further increase the surface warming initially triggered by phytoplankton.

3.3.2 Atmosphere

Figure 6a shows B − A differences in zonally-averaged radiative heat fluxes (shortwave and longwave) and turbulent heat fluxes (latent and sensible) at the Earth's surface, considering both ocean and land. Positive (negative) values indicate downward (upward) heat fluxes. The presence of phytoplankton causes solar radiation incident at the Earth's surface to decrease at tropical latitudes by $\sim$1 W m^{-2} (except on the Equator) and to increase at subtropical and middle latitudes in both hemispheres. Reduced surface solar radiation over the Tropics explains why B − A radiative heating differences are negative in the tropical near-surface ocean (Fig. 3, colors). The B − A changes in shortwave radiation at the Earth's surface are likely linked to changes in cloudiness, which are here estimated by computing the B minus A changes in the difference between "all sky" and "clear sky" shortwave radiation at the Earth's surface, i.e. the shortwave part of the cloud radiative forcing (Fig. 6b). Changes in cloudiness cause shortwave solar radiation at the Earth surface to decrease between 0.5 and 1 W m^{-2} at subpolar-high latitudes and at tropical latitudes (except near the Equator), and to increase at subtropical-middle latitudes. Also changes in vertically-integrated precipitation, which increases by 0.1 mm day^{-1} at tropical latitudes and by 0.05 mm day at subpolar latitudes (i.e. $\sim$5%), are consistent with this pattern. Precipitation and cloudiness changes are tightly linked to changes in strength and position of the Hadley Cell and of the mid-latitude storm tracks (as described in Sect. 3.4). At high latitudes, downward shortwave radiation at the Earth's surface is enhanced in both hemispheres due to the decrease in ocean albedo in the B with respect to the A experiment (Fig. 5c,d).

Latent heat flux differences are negative at all latitudes (−1 W m^{-2} on average) in the B with respect to the A experiment. This arises as a direct response to increased SST which enhances evaporation in the B experiment (not shown). On the other hand, B − A differences in sensible heat fluxes are small but positive at most latitudes. This indicates that in the new energy balance of the B experiment, latent heat fluxes tend to dissipate the SST increase by increasing evaporation, whereas sensible heat fluxes partly counteract this process by providing a heat gain to the ocean.

Increased latent heat losses in the B experiment raise the specific atmospheric humidity by 2–6% almost everywhere with 95% statistical significance. Increased atmospheric humidity reduces the transparency of the Earth's atmosphere thereby causing overall positive B − A differences in longwave radiation at the Earth's surface (up to 1 W m^{-2} over the Tropics). Increased atmospheric water

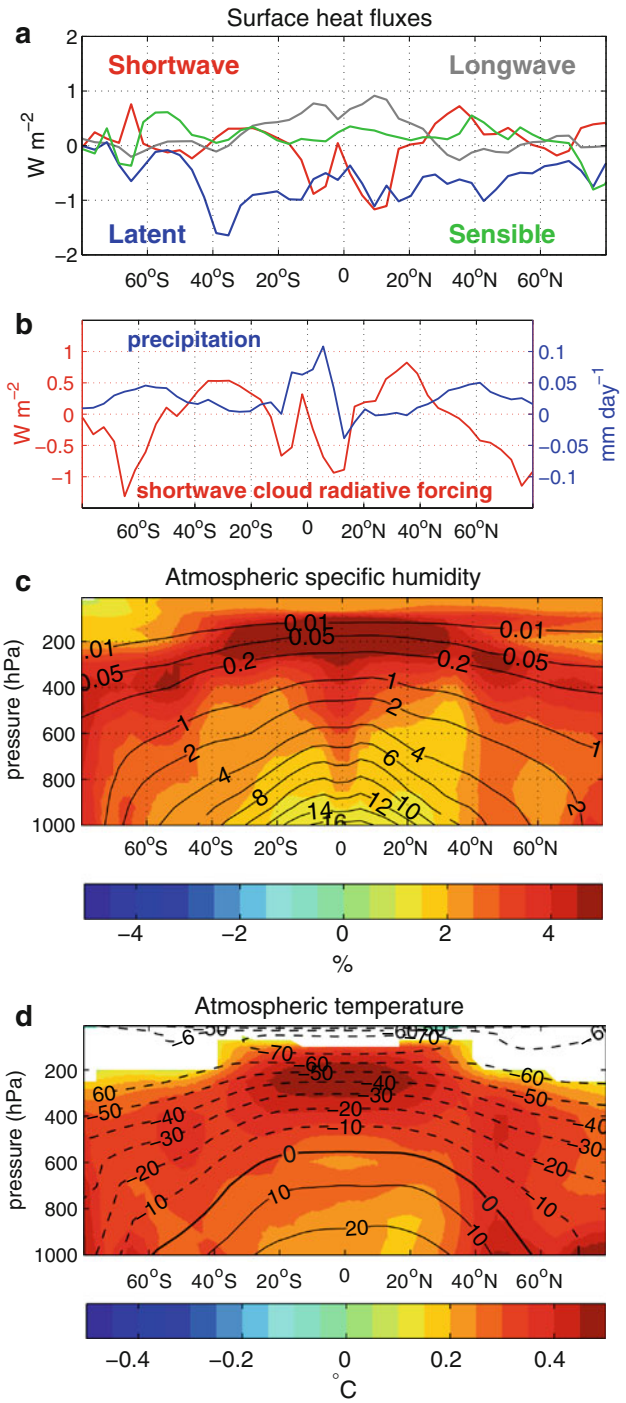

Fig. 6 Zonal averages of **a** $B - A$ differences in heat fluxes in (W m^{-2}) at the Earth's surface, where positive values indicate downward heat fluxes (*red*: shortwave radiation, *grey*: longwave radiation, *blue*: latent heat flux, *green*: sensible heat flux); **b** $B - A$ differences of radiative cloud forcing of shortwave radiation (*red*) at the Earth's surface (W m^{-2}), and of vertically-averaged precipitation in mm day^{-1} (*blue*); **c** $B - A$ percent differences in atmospheric specific humidity (%, calculated as $(B - A)/A \times 100$) in colors and A *experiment* climatology (g/kg) in *contours*, **d** $B - A$ differences in atmospheric temperature (°C) in *colors* and A *experiment* climatology in *contours*. **c** and **d** show only 95% statistically significant $B - A$ differences

vapor enhances the Earth's greenhouse effect (Held and Soden 2000). As a result, atmospheric temperatures increase of up to 0.5°C on zonal and annual average with a statistical significance of 95% (Fig. 6d). The largest changes occur in the tropical upper troposphere as a direct effect of the increased latent heat release. In the stratosphere, B − A differences in atmospheric temperature are slightly negative but not statistically significant. This pattern of temperature increase shows resemblance with the simulated response of atmospheric temperatures to anthropogenic carbon emission scenarios for the 21st century, even though with magnitudes ∼10 times smaller (Meehl et al. 2007).

3.4 Dynamical responses

3.4.1 Atmosphere

Changes in SST induced by phytoplankton affect atmospheric circulation at both tropical and extratropical latitudes. Figure 7 shows the atmospheric mass stream function in the A experiment (in contours) and its changes between experiments B and A (in colors) for December–February (Fig. 7a) and June–August (Fig. 7b). The model simulates two meridional cells composed of ascending motion over the Intertropical Convergence Zone and of descending motion over the Subtropics (the Hadley Cell). In the CGCM, when phytoplankton is allowed to impact the upper-ocean physical structure, the Hadley Cell is weakened and exhibits a poleward widening in both hemispheres. Consistently, atmospheric vertical velocities in the B experiment (not shown) exhibit a 5–10% reduction of ascending motion over the Intertropical Convergence Zone (ITCZ), enhanced ascending motion on the poleward flanks of the ITCZ (owing to the Hadley Cell widening), and increased descending motion at ∼40°N and ∼40°S.

The Hadley Cell weakening and poleward expansion in response to increased atmospheric temperatures resembles the response of most CGCMs when used for global warming projections (Knutson and Manabe 1995; Held and Soden 2006; Lu et al. 2007). The modified vertical atmospheric circulation in the B experiment is likely leading to the changes in shortwave radiative cloud forcing (Fig. 6b) which cause surface shortwave radiation to decrease over the Tropics (except on the Equator) and to increase over the Subtropics (Fig. 6a). Since in the Subtropics attenuation depths for visible radiation in the B experiment are very close to those in the A experiment without biology (Fig. 2c), these domains are expected to be little affected by local biological radiative heating. The subtropical SST increase in the B experiment (Fig. 4d) can instead be due to the teleconnection mechanism provided the Hadley Cell, whose poleward expansion would increase the surface shortwave radiation over the subtropical gyres.

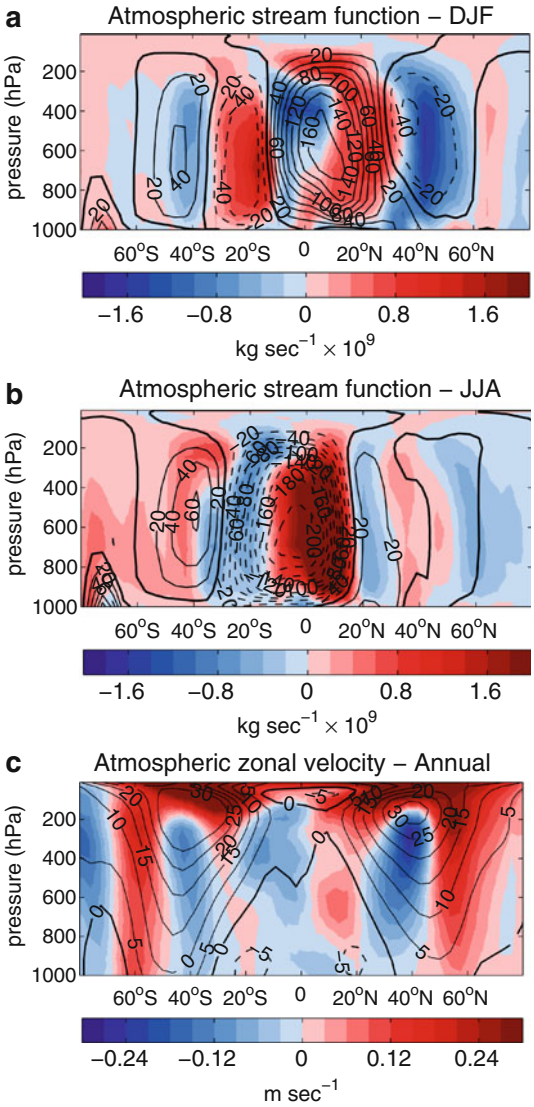

Fig. 7 **a** $B - A$ differences in December–February (DJF) atmospheric meridional overturning stream function (10^9 kg s^{-1}) in *colors* and *A experiment* DJF climatology in *contours* (spacing 25×10^9 kg s^{-1}), where positive (negative) values indicate clockwise (anticlockwise) motion; **b** same as **a** but for June–August (JJA); **c** zonal averages of $B - A$ differences in atmospheric zonal velocities (m s^{-1}) in *colors* and *A experiment* annual climatology in *contours* (spacing 5 m s^{-1}), where positive (negative) values indicate westerly (easterly) winds

At middle and subpolar latitudes, phytoplankton causes up to 5% changes in mean zonal winds (Fig. 7c). In particular, extratropical westerly winds in the B experiment are weaker at middle latitudes (around 40°N and 40°S) and stronger at subpolar latitudes (around 60°N and 60°S). This pattern is indicative of a poleward shift of mid-latitude westerly winds in the B with respect to the A experiment. Two explanations for this poleward shift can be invoked. First, the poleward shift is consistent with the weakening and poleward expansion of the Hadley Cell in warmer

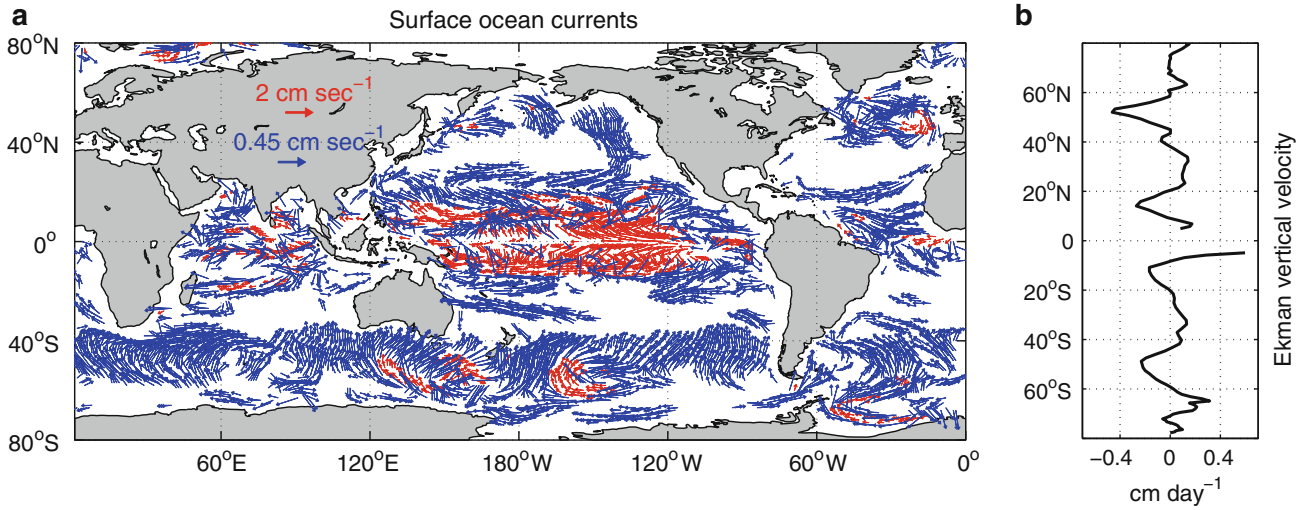

Fig. 8 **a** $B - A$ differences in surface ocean currents (cm s^{-1}), where a different scaling is used for velocity differences larger than 0.45 cm s^{-1} (*red*) and included between 0.15 and 0.45 cm s^{-1} (*blue*); velocities lower than 0.15 cm s^{-1} are not shown; **b** zonal averages of $B - A$ differences of Ekman ocean vertical velocities (cm day^{-1}), where positive (negative) values indicate upward (downward) vertical velocities

tropical conditions (Schneider 1984). Second, the two experiments differ in their atmospheric meridional baroclinicity, which affects the vertical shear of zonal winds through the thermal wind relation. The largest increase in atmospheric temperature (Fig. 6c) and SST (Fig. 4d) in the B experiment occurs at middle latitudes: this decreases meridional temperature gradients between subtropical and middle latitudes and increases them between middle and polar latitudes. As a result, the vertical shear of zonal winds is reduced (enhanced) equatorward (poleward) of $\sim 45°$. When integrated throughout the atmospheric column, these changes in zonal wind shear are associated with a poleward shift of mid-latitude westerly winds in the B experiment. In the upper troposphere, the increase in tropical-extratropical temperature gradients (Fig. 6c) causes an intensification of the westerly wind component.

3.4.2 Ocean

Figure 8a shows B − A differences in surface ocean circulation, where a different scaling is used for velocity differences larger than 0.45 cm s^{-1} and included between 0.15 and 0.45 cm s^{-1} (differences smaller than 0.15 cm s^{-1} are not shown). The largest surface velocity changes occur in the central equatorial Pacific, where the B experiments shows a strengthening of the equatorial divergence and of the Southern Equatorial Current by 1–2 cm s^{-1} (i.e. 5% of absolute values). Figure 8b shows mean B − A differences in Ekman vertical velocities, computed as the curl of the wind stress divided by mean seawater density and the Coriolis parameter ($f = 2\Omega \sin \varphi$, where Ω is the Earth's angular velocity and φ is latitude). In the Tropical belt, B − A differences of Ekman vertical velocities are positive with values of 0.5 cm day^{-1} ($\sim 5\%$ of the absolute values). The positive differences correspond to an increased cyclonic vorticity input by the wind stress curl, which in turn enhances equatorial divergence and upper-ocean upwelling (not shown). As it can be seen in Fig. 9a (red), the increased equatorial Pacific divergence in the B experiment enhances the poleward oceanic heat transport by about 0.05 PW (1 PW = 10^{15} W), i.e. $\sim$ 5% of absolute values, in the equatorial belt between 10°S and 10°N.

In the subpolar North Atlantic and North Pacific Oceans, the poleward shift of westerly winds in the B experiment gives rise to anticyclonic wind stress curl anomalies and anomalous downward Ekman vertical velocities (Fig. 8b). As a response to these wind changes, B − A differences in surface ocean circulation show a poleward shift of the North Atlantic Current and of the North Pacific Current. The arising anticyclonic ocean circulation anomaly is geostrophically adjusted to the mid-latitude ocean temperature increases occurring in the B experiment (Fig. 4b,c). The ocean velocity differences between the two experiments are about 0.45 cm s^{-1}, i.e. about 5% of absolute values. The changes in the wind-driven circulation occurring in the B experiment also affect the North Atlantic meridional overturning circulation (MOC) stream function (Fig. 9b). The MOC stream function in the A experiment exhibits northward transport in the upper 1,000 m depth and southward transport between 1,000 and 3,000 m depth, with a maximum transport of 11 Sv (1 Sv=10^6 m^3 s^{-1}) at 30°N. This value is at the weaker end—even though within the range—of other CGCM estimates (Fig. 10.15 in Meehl et al. 2007). In the B experiment, the MOC is strengthened

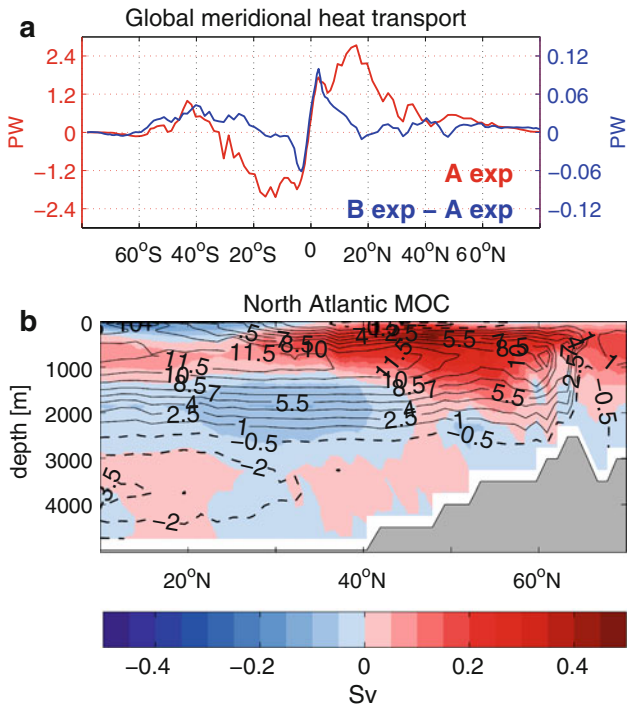

Fig. 9 **a** Annually-averaged global meridional ocean heat transport in the *A experiment* (*red curve*) and $B - A$ differences (*blue curve*), where positive (negative) values in the northern (southern) hemisphere indicate poleward heat transport; **b** annually-averaged North Atlantic meridional overturning circulation (MOC) stream function (Sv) in the *A experiment* in *contours* (spacing 1.5 Sv) and $B - A$ differences in *colors*

in the upper 1,000 m by up to 0.5 Sv at 50°N (i.e. 5–10%) and weakened underneath by about 0.2 Sv at 30°N. These changes are indicative of an upward and northward shift of the MOC. This arises as a wind-driven response to the poleward intensified westerly winds (Eden and Willebrand 2001) and is associated with a deepening of the winter MLD in the Nordic Seas (not shown) indicating an intensification of the northernmost site of North Atlantic deep water formation in the coupled model. As it will be discussed in Sect. 6, this result is not totally in agreement with the study of Lengaigne et al. (2009) who instead detect a 2 Sv weakening of the MOC when phytoplankton is present.

In the Southern Ocean, the equatorward surface circulation is enhanced in the B with respect to the A experiment (Fig. 8a). This is consistent with the poleward intensification of westerly winds in the B experiment, which causes negative Ekman vertical velocities between 40 and 60°S (Fig. 8b) and increased northward Ekman transport. This response is typical of coupled climate model simulations at this resolution (Fyfe and Saenko 2006). As a response to the increased equatorward circulation in the B experiment, the poleward heat transport in the Southern Ocean is reduced by 0.03 PW (i.e. 5% of absolute values).

3.5 Synthesis

A better understanding of the role of different dynamical responses triggered by phytoplankton may be obtained by analyzing the separate contribution of the heat trend terms in the ocean temperature heat equation. In addition to the radiative heating term described in Eq. 2, the other terms analyzed here are temperature advection by zonal, meridional and vertical ocean circulation. These terms are vertically integrated in the first 300 m of the water column and averaged horizontally over the major ocean basins, i.e. Tropical Pacific Ocean, Tropical Atlantic Ocean, Tropical Indian Ocean, North Pacific Ocean, North Atlantic Ocean, and subpolar Southern Ocean. Table 2 shows, for both experiments, the averages over the last 100 years of these terms together with the standard deviation of their annual means, whereas Fig. 10 shows the $B - A$ differences for each basin. The aim here is not to construct a heat budget of each region, which is beyond the scope of this study, but to better quantify the interplay of different physical responses triggered by phytoplankton.

In the Tropical Oceans, upper-ocean radiative heating in the B experiment exhibits a decrease between 0.5 and 1 W m^{-2}. This change is caused by decreased surface solar radiation, related to the increase in cloud radiative forcing and precipitation (Fig. 6b). The B experiment also exhibits an increase in vertical advective cooling of the upper ocean due to increased upwelling (not shown) driven by increased equatorial divergence (Fig. 8a). However, the vertical advective cooling is balanced by increased horizontal advective heating caused by stronger Equatorial Undercurrents and by a spin-up of the shallow meridional overturning cells (not shown). In the Tropical Atlantic, the vertical advective cooling in the B experiment is smaller than in the other tropical basins and is mostly balanced by meridional advective warming.

The North Pacific and North Atlantic Oceans are both characterized by higher upper-ocean radiative heating (up to 0.9 W m^{-2}) in the B with respect to the A experiment, owing to higher surface solar radiation at subtropical latitudes (Fig. 6a). The B experiment also exhibits a larger upper-ocean heating by meridional advection. In particular in the North Atlantic, meridional advective heating in the upper ocean increases by 2 W m^{-2}, consistent with the intensification of the upper branch of the North Atlantic MOC (Fig. 9b). In the Southern Ocean, the B experiment cools by $\sim$0.7 W m^{-2} because of increased vertical advection. This is caused by increased upwelling (not shown) necessary to balance the increased northward Ekman transport (Fig. 8a).

The $B - A$ differences in heating terms (Fig. 10) are in general lower, even though of similar magnitude, as the standard deviations of their annual means (Table 2). This

Table 2 Annually-averaged heat trend terms (W m^{-2}) integrated over the first 300 m depth and their standard deviations in the B and A experiments. Considered here are radiative heating (column 2), zonal advective heating (column 3), meridional advective heating (column 4), and vertical advective heating (column 5). Terms are horizontally averaged over the North Atlantic (30–65°N, 70°W–20°E), North Pacific (30°–60°N, 130°E–100°W), subpolar Southern Ocean (50–70°S, 180°W–180°E), Tropical Pacific (20°S–20°N, 130°E–80°W), Indian Ocean (25°S–25°N, 40–120°E), and Tropical Atlantic (25°S–25°N, 60°W–30°E)

	Radiative heating	Zonal advection	Meridional advection	Vertical advection
North Atlantic	A = 115.09 ± 1.38	A = −6.16 ± 2.77	A = 18.00 ± 3.12	A = 3.76 ± 0.84
	B = 115.53 ± 1.48	B = −7.61 ± 2.87	B = 20.04 ± 3.32	B = 3.69 ± 0.93
North Pacific	A = 118.53 ± 1.77	A = 5.13 ± 2.23	A = 14.09 ± 3.71	A = 2.58 ± 1.23
	B = 119.45 ± 1.73	B = 4.75 ± 1.98	B = 14.68 ± 2.91	B = 2.23 ± 1.28
Southern Ocean	A = 62.87 ± 0.75	A = −8.99 ± 0.41	A = 0.38 ± 2.22	A = −1.38 ± 0.99
	B = 63.13 ± 0.72	B = −9.33 ± 0.45	B = 0.55 ± 2.42	B = −2.12 ± 0.94
Tropical Pacific	A = 225.57 ± 2.52	A = 10.98 ± 4.46	A = 44.49 ± 4.18	A = −83.63 ± 4.59
	B = 224.48 ± 2.71	B = 12.27 ± 4.67	B = 45.19 ± 4.65	B = −85.50 ± 4.84
Indian Ocean	A = 212.81 ± 1.70	A = −9.42 ± 2.14	A = 60.47 ± 3.49	A = −60.22 ± 3.83
	B = 211.79 ± 1.64	B = −8.29 ± 2.17	B = 60.12 ± 3.16	B = −60.90 ± 3.99
Tropical Atlantic	A = 224.30 ± 1.27	A = 3.94 ± 1.89	A = 33.72 ± 1.87	A = −55.89 ± 2.95
	B = 223.74 ± 1.51	B = 3.88 ± 2.27	B = 34.08 ± 2.07	B = −56.11 ± 2.94

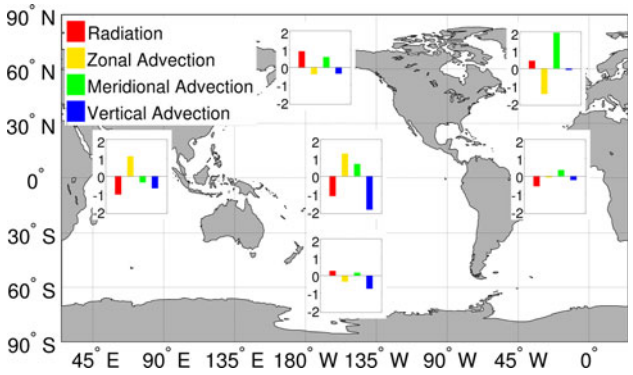

Fig. 10 $B - A$ differences in the ocean heat trend terms integrated over the first 300 m depth (W m^{-2}) and horizontally averaged over the North Pacific (30–60°N, 130°E–100°W), the North Atlantic (30–65°N, 70°W–20°E), the Indian Ocean (25°S–25°N, 40–120°E), the Tropical Pacific (20°S–20°N, 130°E–80°W), the Tropical Atlantic (25°S–25°N, 60°W–20°E), and the subpolar Southern Ocean (50–70°S, 180°W–180°E). *Red*: radiative heat trend, *yellow*: zonal advective heat trend, *green*: meridional advective heat trend, *blue*: vertical advective heat trend

result indicates that in this model the influence of phytoplankton on physical climate properties are within the range of natural climate variability.

4 Discussion and conclusions

In this study, the climate responses to phytoplankton solar radiation absorption are investigated by using a coupled ocean–atmosphere model containing a complex marine biogeochemistry model. Phytoplankton causes an increase of solar radiation absorption in the near-surface ocean, and is found to increase SST by ~0.3–0.5°C throughout most of the global ocean. This gives rise to several coupled ocean–atmosphere responses which may alternatively enhance or damp the phytoplankton near-surface heating. From this study, four pathways are identified by which the SST changes caused by phytoplankton may influence global climate properties (as schematically summarized in Fig. 11):

1. The global increase in SST enhances latent heat losses and evaporation from the ocean. This increases atmospheric water vapor, thereby enhancing the Earth's greenhouse effect and atmospheric temperatures (positive effect on global SST).
2. The high-latitude increase in SST reduces sea-ice cover and albedo, thereby increasing the quantity of solar radiation absorbed by the ocean (positive effect onto high-latitude SSTs).
3. The poleward expansion of the Hadley Cell enhances cloudiness and reduces surface shortwave radiation over the Tropics except on the Equator (negative effect on tropical SST) and increases surface shortwave radiation at subtropical latitudes (positive effect on subtropical SST). Furthermore, increased cyclonic wind vorticity over the Tropics enhances equatorial oceanic divergence and upwelling (negative effect on equatorial SST).
4. Changes in the atmospheric baroclinicity cause a poleward shift of mid-latitude westerly winds in both hemispheres. As a result, the North Atlantic MOC extends more northward (positive effect on subpolar

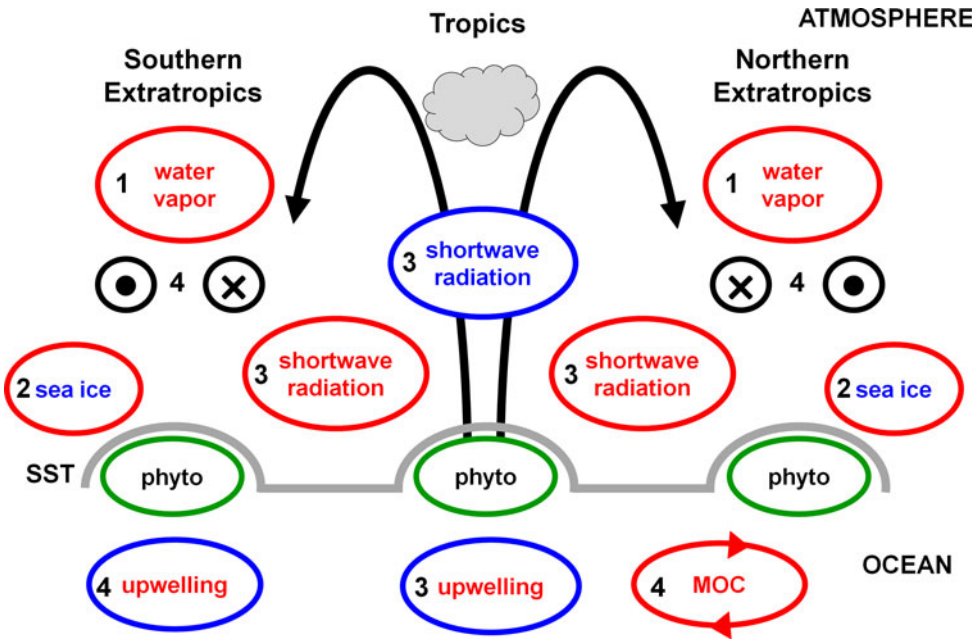

Fig. 11 Schematic representation (as emerging from this study) of the global impacts triggered by phytoplankton (CHL) and by its associated increase in SST (*grey line*). *Red* (*blue*) words indicate a property strengthening (weakening) and *red* (*blue*) *circles* indicate whether this change exerts a positive (negative) effect on SST. (1) Enhanced ocean latent heat losses increase atmospheric water vapor, thereby enhancing the Earth's greenhouse effect; (2) reduced sea-ice cover and albedo enhance the quantity of solar heat absorbed by the ocean; (3) the poleward expansion of the Hadley Cell (*black curve*) increases cloudiness over the Tropics and reduces it at subtropical latitudes; increased cyclonic wind vorticity in the Tropics enhances equatorial divergence and upwelling; (4) changes in the atmospheric baroclinicity cause a poleward shift of mid-latitude westerly winds in both hemispheres (*black dots* and *crosses*): this causes a northward shift of the North Atlantic MOC and an enhancement of the Southern Ocean upwelling

SST) and in the Southern Ocean the equatorward Ekman transport and the upwelling are enhanced (negative effect on subpolar SST).

Globally, phytoplankton leads to an upper-ocean heat content increase of $\sim 1 \times 10^8$ J m^{-2}. Regionally however, the combination of atmospheric and oceanic responses depict a clear pattern of reduced ocean heat content in the Tropics, enhanced ocean heat content at subtropical-middle latitudes, and reduced ocean heat content in the subpolar Southern Ocean. This study therefore suggests that phytoplankton radiative heating may reduce the tropical-extratropical gradient of upper-ocean heat content.

Biases in the simulated chlorophyll distribution should however be considered when interpreting the results. For instance, it can be envisaged that the lower-than-observed chlorophyll concentration in the subtropical gyres (and higher-than-observed chlorophyll concentration in the Southern Ocean) may lead to an overestimated gradient of B − A SST differences and thus to an overestimated poleward intensification of westerly winds. Also, in the North Atlantic the chlorophyll underestimation may reduce the sea ice response to phytoplankton.

This and previous studies agree fairly well in finding that northern extratropical latitudes are warmed by local phytoplankton heating (Oschlies 2004; Manizza et al. 2005, 2008; Wetzel et al. 2006; Lengaigne et al. 2009), even though the magnitude of the warming varies somewhat between studies. For instance, in this model the mid-latitude warming is larger with respect to the OGCM studies of Oschlies (2004) and Manizza et al. (2008). Indeed, in this study the extratropical SST increase is particularly large due to coupled-ocean atmosphere feedbacks, which are not captured within ocean-only configurations. As previously mentioned, the intensification of the upper branch of the North Atlantic MOC does not wholly agree with the CGCM study by Lengaigne et al. (2009), who instead detect a reduction of the MOC transport when phytoplankton is present (due to increased sea ice melting, runoff and precipitation which reduce North Atlantic salinity). In the CGCM used in this study, runoff is climatologically prescribed and the surface freshwater balance in response to phytoplankton is dominated by the increased evaporative losses which enhance North Atlantic sea surface salinity (not shown). This result draws attention on how sensitively the North Atlantic MOC simulated by CGCMs responds to small changes in the magnitude and spatial patterns of freshwater fluxes. A large spread in the MOC responses among different CGCMs is indeed well-known also among IPCC climate models forced with the A1B anthropogenic climate change scenario (Meehl et al. 2007).

Existing modeling studies show a large spread in the Tropical Pacific SST response to phytoplankton. This is likely due to the widely varying modeling strategies used in different studies, which makes the systematic comparison among results complicated. Some pattern is however visible, and three groups of modeling frameworks obtaining comparable results are identified:

1. This study and those by Wetzel et al. (2006) and Lengaigne et al. (2007), which similarly use a CGCM containing interactive marine biogeochemistry, all simulate an increase in eastern equatorial SST of $\sim$0.5°C when marine biogeochemistry is present. Lengaigne et al. (2007) and this study are consistent also in the depth structure of ocean temperature changes (near-surface warming and subsurface cooling) which highlights the local effect of phytoplankton radiative heating. Also, both studies show that the coupling with the atmosphere tend to amplify the warming due to phytoplankton in the equatorial Pacific, either because of weakened trade winds (Lengaigne et al. 2007) or because of enhanced atmospheric water vapor feedback (this study).
2. A number of OGCM studies (Nakamoto et al. 2001; Manizza et al. 2005, 2008; Löptien et al. 2009) detect a cooling of equatorial Pacific SST due to ocean circulation changes triggered by phytoplankton. However, in the light of this and previous CGCM studies, it can be argued that OGCM studies may not be capable of simulating the full climate response to phytoplankton, since they lack the coupling with the atmosphere which is particularly relevant in the Tropics.
3. The studies by Anderson et al. (2007) and Gnanadesikan and Anderson (2009), which use a CGCM forced with prescribed attenuation depths from SeaWiFS satellite data, detect a reduction of equatorial Pacific SST when phytoplankton is present. These studies show that shallower attenuation depths in the oligotrophic subtropical gyres cause equatorward entrainment of relatively cooler subsurface waters within the shallow meridional overturning cells. There are two points which may help to interpret the discrepancy between our results and those from Gnanadesikan and Anderson (2009). First, this model exhibits off-equatorial deep chlorophyll maxima at $\sim$80 m depth, in agreement with observations (Conkright et al. 2002). The equatorward closure of the shallow meridional overturning cells ($\sim$60 m depth in this model) is above the subsurface cooling maximum caused by phytoplankton. Were we to apply vertically-constant attenuation depths (as in Gnanadesikan and Anderson 2009) our B − A radiative heating profiles would likely be shifted upwards, and the equatorward flow would entrain more biologically-cooled waters. Second, since this model underestimates chlorophyll concentrations in the subtropical gyres, off-equatorial regions experience less phytoplankton-related subsurface cooling than in reality. It is thus likely that in this model the subsurface waters advected towards the equator are relatively warmer compared to a more realistic condition of higher chlorophyll.

A question is whether it is worth adding biogeochemistry to climate models in order to simulate the effect of phytoplankton radiative heating on global climate. Quantitatively, in this study the changes in physical properties caused by phytoplankton are generally (1) more than an order of magnitude smaller than the typical error of "physical-core-only" climate models (Randall et al. 2007)—and it is to be remarked that the addition of biogeochemistry does not improve the physics of the coupled model—(2) almost an order of magnitude smaller than the projected impacts of anthropogenic climate change in 21st century climate model projections (Meehl et al. 2007), (3) of comparable amplitude with respect to the natural variability of the climate system. Another question is the level of biogeochemical complexity needed in order to correctly capture the phytoplankton influence on climate. This study suggests that the horizontal and vertical structure of chlorophyll is relevant and that the use of satellite data to prescribe vertically-constant attenuation depths may lead to different results. However, a simple biogeochemical model, capable of simulating the major large-scale chlorophyll patterns, could be a more computationally-efficient alternative to the complex biogeochemical model used in this study. Finally, another question is how long the simulations should be in order to investigate the climate response to phytoplankton radiative heating. In this model upper-ocean heat content takes at least 100 years to adjust to phytoplankton. If this is true for other CGCMs, analyses performed on shorter simulations may lead to different results.

This study shows that the atmospheric response to phytoplankton solar absorption resembles in many respects the so-called "robust response" of CGCMs to increased greenhouse gases and tropospheric warming, including increased precipitation over the Tropics, weakening of the Hadley Cell, poleward displacement of mid-latitude westerlies, and warming of the upper troposphere (Held and Soden 2006; Lorenz and DeWeaver 2007; Lu et al. 2007). This is likely due to similarities in the water vapor increase which in this case is triggered by phytoplankton heating in the upper ocean.

This study illustrates how phytoplankton solar radiation absorption affects physical climate properties in the adjusted state of a fully coupled ocean–atmosphere

simulation. Several of these physical changes indeed represent environmental modifications of relevance for phytoplankton growth, thereby empowering potential regulatory feedback loops between climate and phytoplankton. The available experiments do not allow quantifying the feedback of phytoplankton heating onto itself; nevertheless this study suggests possible pathways through which phytoplankton may regulate its abundance through positive and negative climate feedbacks. At subtropical and middle latitudes, this and previous ocean-only studies (Oschlies 2004; Manizza et al. 2008) show that phytoplankton radiative heating increases SST by 0.5–1°C. In a previous study performed with the B experiment, marine biogeochemistry has been demonstrated to respond to natural fluctuations in North Atlantic surface ocean conditions in some predictable ways (Patara et al. 2011). A SST increase of 0.5–1°C was found to be associated with a chlorophyll decrease of around 0.05–0.1 mg m^{-3}, because of reduced mixing and nutrient supply. By combining the results from Patara et al. (2011) with those shown here, it can be estimated that phytoplankton abundance at middle latitudes is controlled by a negative feedback, whose order of magnitude is in good agreement with the studies of Oschlies (2004) and Manizza et al. (2008), where the phytoplankton feedback was explicitly assessed. At high-latitudes, where phytoplankton growth is mostly limited by sunlight, the reduction in sea ice triggered by phytoplankton, also found by Manizza et al. (2008), would allow more sunlight penetration and would thus favor higher phytoplankton growth (Oschlies 2004), thus acting as a positive feedback as long as sea ice is present. In the upwelling regions of the Southern Ocean and of the equatorial Pacific, this study suggests that the presence of phytoplankton may trigger an increase of the wind-driven upwelling which is likely to increase nutrient supply and to favor phytoplankton growth.

At a global scale, phytoplankton is suggested to increase SST by $\sim$0.2°C, thereby enhancing atmospheric water vapor and atmospheric temperatures. There is increasing evidence that enhanced atmospheric temperatures may reduce phytoplankton productivity and chlorophyll concentrations because of enhanced ocean stratification (Behrenfeld et al. 2006; Falkowski and Oliver 2007), even though this issue is still a matter of debate (Sarmiento et al. 2004; Boyce et al. 2010). If increased atmospheric temperatures were to globally damp the phytoplankton abundance, this would increase ocean clarity and reduce the biological increase in SST, in water vapor and in atmospheric temperatures. This would constitute a negative feedback loop connecting phytoplankton abundance and the Earth's greenhouse effect. This hypothesis suggests the relevance of phytoplankton as an internal constituent of the Earth's climate and its potential role in participating in long-term climate adjustment. As yet the quantification of this phytoplankton-climate feedback remains a key question to be addressed in future studies, in order to better understand the nature of the Earth System feedbacks and the role of phytoplankton therein.

Acknowledgments This study was funded by Centro Euro-Mediterraneo per i Cambiamenti Climatici (CMCC). The authors thank the European Centre for Medium-Range Weather Forecasts (ECMWF) for making available ERA-40 wind stress data, the US National Aeronautics and Space Administration (NASA) for providing SeaWiFS chlorophyll satellite products, and the Hadley Centre for the sea surface temperature data available on the website http://www.metoffice.gov.uk/hadobs. The authors thank E. Schneider for his comments on a previous version of the manuscript. Two anonymous reviewers are also gratefully acknowledged.

References

Anderson WG, Gnanadesikan A, Hallberg R, Dunne J, Samuels BL (2007) Impact of ocean color on the maintenance of the Pacific Cold Tongue. Geophys Res Lett. doi:10.1029/2007GL030100

Anderson W, Gnanadesikan A, Wittenberg A (2009) Regional impacts of ocean color on tropical Pacific variability. Ocean Science 5(3):313–327

Behrenfeld MJ, O'Malley RT, Siegel DA, McClain CR, Sarmiento JL, Feldman GC, Milligan AJ, Falkowski PG, Letelier RM, Boss ES (2006) Climate-driven trends in contemporary ocean productivity. Nature 444(7120):752–755

Blanke B, Delecluse P (1993) Variability of the Tropical Atlantic Ocean simulated by a general circulation model with 2 different mixed-layer physics. J Phys Oceanogr 23(7):1363–1388

Boyce DG, Lewis MR, Worm B (2010) Global phytoplankton decline over the past century. Nature 466(7306):591–596

Conkright M, Garcia H, O'Brien T, Locarnini R, Boyer T, Stephens C, Antonov J (2002) World Ocean Atlas 2001, vol 4: Nutrients. In: NOAA Atlas NESDIS 52, US Government Printing Office, Washington DC

Eden C, Willebrand J (2001) Mechanisms of interannual to decadal variability in the North Atlantic circulation. J Climate 14:2266–2280

Falkowski PG, Oliver MJ (2007) Mix and match: how climate selects phytoplankton. Nat Rev Microbiol 5:813–819. doi:10.1038/nrmicro1751

Fogli PG, Manzini E, Vichi M, Alessandri A, Patara L, Gualdi S, Scoccimarro E, Masina S, Navarra A (2009) INGV-CMCC Carbon (ICC): A Carbon Cycle Earth System Model. CMCC Research Paper 61. http://www.cmcc.it/publications-meetings/publications/research-papers/rp0061-ans-04-2009

Fortuin JPF, Kelder H (1998) An ozone climatology based on ozonesonde and satellite measurements. J Geophys Res 103(D24):31709–31734. doi:10.1029/1998JD200008

Fyfe JC, Saenko OA (2006) Simulated changes in the extratropical Southern Hemisphere winds and currents. Geophys Res Lett 33:L06701. doi:10.1029/2005GL025332

Garcia HE, Locarnini RA, Boyer TP, Antonov JI, Zweng MM, Baranova OK, Johnson DR (2010) World Ocean Atlas 2009, Volume 4: Nutrients (phosphate, nitrate, silicate). In: Levitus S (ed) NOAA Atlas NESDIS 71, U.S. Government Printing Office, Washington, DC

Geider RJ, MacIntyre HL, Kana TM (1997) Dynamic model of phytoplankton growth and acclimation: Responses of the balanced growth rate and the chlorophyll a : carbon ratio to

light, nutrient-limitation and temperature. Mar Ecol Progr Ser 148(1–3):187–200
Gent PR, McWilliams JC (1990) Isopycnal mixing in ocean circulation models. J Phys Oceanogr 20(1):150–155
Gnanadesikan A, Anderson WG (2009) Ocean Water Clarity and the Ocean General Circulation in a Coupled Climate Model. J Phys Oceanogr 39(2):314–332
Gnanadesikan A, Emanuel K, Vecchi GA, Anderson WG, Hallberg R (2010) How ocean color can steer Pacific tropical cyclones. Geophys Res Lett 37:L18802. doi:10.1029/2010GL044514
Held IM, Soden BJ (2000) Water vapor feedback and global warming. Annual Review of Energy and the Environment 25:441–475
Held IM, Soden BJ (2006) Robust responses of the hydrological cycle to global warming. J Clim 19(21):5686–5699. doi:10.1175/JCLI3990.1
Jerlov NG (1968) Optical oceanography. American Elsevier Publ. Co., Inc., New York
Jochum M, Yeager S, Lindsay K, Moore K, Murtugudde R (2010) Quantification of the Feedback between Phytoplankton and ENSO in the Community Climate System Model. J Climate 23(11):2916–2925
Johns TC, Royer J-F, Höschel I, Huebener H, Roeckner E, Manzini E, May W, Dufresne J-L, Otterå OH, van Vuuren DP, Salas y Melia D, Giorgetta M, Denvil S, Yang S, Fogli PG, Körper J, Tjiputra JF, Stehfest E, Hewitt CD (2011) Climate change under aggressive mitigation: the ENSEMBLES multi-model experiment. Clim Dyn 37(9–10):1975–2003. doi:10.1007/s00382-011-1005-5
Key RM, Kozyr A, Sabine CL, Lee K, Wanninkhof R, Bullister JL, Feely RA, Millero FJ, Mordy C, Peng TH (2004) A global ocean carbon climatology: Results from global data analysis project (GLODAP). Glob Biogeochem Cyc 18:GB4031. doi:10.1029/2004GB002247
Knutson TR, Manabe S (1995) Time-mean response over the Tropical Pacific to increased CO_2 in a coupled ocean-atmosphere model. J Clim 8(9):2181–2199. doi:10.1175/1520-0442(1995)008<2181:TMROTT>2.0.CO;2
Lengaigne M, Menkes C, Aumont O, Gorgues T, Bopp L, Andre JM, Madec G (2007) Influence of the oceanic biology on the tropical Pacific climate in a coupled general circulation model. Clim Dyn 28(5):503–516
Lengaigne M, Madec G, Bopp L, Menkes C, Aumont O, Cadule P (2009) Bio-physical feedbacks in the Arctic Ocean using an Earth System Model. Geophys Res Lett 36:L21602. doi:10.1029/2009GL040145
Levitus S, Boyer T, Conkright M, O'Brien T, Antonov J, Stephens C, Stathoplos L, Johnson D, Gelfeld R (1998) World Ocean Database 1998: vol. 1: Introduction. In: NOAA Atlas NESDIS 18, p 346, U.S. Gov. Printing Office, Washington, DC
Löptien U, Eden C, Timmermann A, Dietze H (2009) Effects of biologically induced differential heating in an eddy-permitting coupled ocean-ecosystem model. J Geophys Res Oceans 114:C06011. doi:10.1029/2008JC004936
Lorenz DJ, DeWeaver ET (2007) Tropopause height and zonal wind response to global warming in the IPCC scenario integrations. J Geophys Res 112:D10119. doi:10.1029/2006JD008087
Lu J, Vecchi GA, Reichler T (2007) Expansion of the Hadley cell under global warming. Geophys Res Lett 34(6):L06805. doi:10.1029/2006GL028443
Madec G, Imbard M (1996) A global ocean mesh to overcome the North Pole singularity. Clim Dyn 12(6):381–388
Madec G, Delecluse P, Imbard M, Levy C (1998) OPA 8.1 Ocean General Circulation Model Reference Manual. Note du Pole de Modélisation, 11, Institut Pierre Simon Laplace, Paris
Manizza M, Le Quéré C, Watson AJ, Buitenhuis ET (2005) Bio-optical feedbacks among phytoplankton, upper ocean physics and sea-ice in a global model. Geophys Res Lett 32:L05603. doi:10.1029/2004GL020778
Manizza M, Le Quéré C, Watson AJ, Buitenhuis ET (2008) Ocean biogeochemical response to phytoplankton-light feedback in a global model. J Geophys Res-Oceans 113:C10010. doi:10.1029/2007JC004478
Marzeion B, Timmermann A, Murtugudde R, Jin FF (2005) Biophysical feedbacks in the tropical Pacific. J Climate 18(1):58–70
McClain CR (2009) A Decade of Satellite Ocean Color Observations. Annual Review of Marine Science 1:19–42
Meehl GA, Stocker TF, Collins P, Friedlingstein WD, Gaye AT, Gregory JM, Kitoh A, Knutti R, Murphy JM, Noda A, Raper SCB, Watterson IG, Weaver AJ, Zhao ZC (2007) Global Climate Projections. In: Solomon S, Qin D, Manning M, Chen Z, Marquis M, Averyt KB, Tignor M, Miller HL (eds) Climate Change 2007: The Physical Science Basis. Cambridge University Press, Cambridge, United Kingdom and New York, NY, USA, Contribution of Working Group I to the Fourth Assessment Report of the Intergovernmental Panel on Climate Change
Morel A, Antoine D (1994) Heating rate within the upper ocean in relation to its bio-optical state. J Phys Oceanogr 24(7):1652–1665
Murtugudde R, Beauchamp J, McClain CR, Lewis M, Busalacchi AJ (2002) Effects of penetrative radiation on the upper tropical ocean circulation. J Climate 15(5):470–486
Nakamoto S, Kumar SP, Oberhuber JM, Ishizaka J, Muneyama K, Frouin R (2001) Response of the equatorial Pacific to chlorophyll pigment in a mixed layer isopycnal ocean general circulation model. Geophys Res Lett 28(10):2021–2024
Oschlies A (2004) Feedbacks of biotically induced radiative heating on upper-ocean heat budget, circulation, and biological production in a coupled ecosystem-circulation model. J Geophys Res Oceans 109:C12031. doi:10.1029/2004JC002430
Patara L, Visbeck M, Masina S, Krahmann G, Vichi M (2011) Marine biogeochemical responses to the North Atlantic Oscillation in a coupled climate model. J Geophys Res 116:C07023. doi:10.1029/2010JC006785
Paulson CA, Simpson JJ (1977) Irradiance measurements in upper ocean. J Phys Oceanogr 7(6):952–956
Randall DA, Wood RA, Bony S, Colman R, Fichefet T, Fyfe J, Kattsov V, Pitman A, Shukla J, Srinivasan J, Stouffer RJ, Sumi A, Taylor KE (2007) Climate Models and Their Evaluation. In: Solomon S, Qin D, Manning M, Chen Z, Marquis M, Averyt KB, Tignor M, Miller HL (eds) Climate Change 2007: The Physical Science Basis. Cambridge University Press, Cambridge, United Kingdom and New York, NY, USA, Contribution of Working Group I to the Fourth Assessment Report of the Intergovernmental Panel on Climate Change
Rayner NA, Parker DE, Horton EB, Folland CK, Alexander LV, Rowell DP, Kent EC, Kaplan A (2003) Global analyses of sea surface temperature, sea ice, and night marine air temperature since the late nineteenth century. J Geophys Res 108:4407. doi:10.1029/2002JD002670
Röckner E, Bäuml G, Bonaventura L, Brokopf R, Esch M, Giorgetta M, Hagemann S, Kirchner I, Kornblueh L, Manzini E, Rhodin A, Schlese U, Schulzweida U, Tompkins A (2003) The atmospheric general circulation model ECHAM5, Part I: Model description. Max-Planck-Institute for Meteorology, Report No. 349, Hamburg, Germany
Russell JL, Stouffer RJ, Dixon KW (2006) Intercomparison of the Southern Ocean circulations in IPCC coupled model control simulations. J Climate 19(18):4560–4575
Sarmiento JL, Slater R, Barber R, Bopp L, Doney SC, Hirst AC, Kleypas J, Matear R, Mikolajewicz U, Monfray P, Soldatov V, Spall SA, Stouffer R (2004) Response of ocean ecosystems to climate warming. Glob Biogeochem Cy 18 (3): Art. No. GB3003

Sathyendranath S, Gouveia AD, Shetye SR, Ravindran P, Platt T (1991) Biological-control of surface-temperature in the Arabian Sea. Nature 349(6304):54–56

Schneider EK (1984) Response of the annual and zonal mean winds and temperatures to variations in the heat and momentum sources. J Atmos Sci 41:1093–1115

Schneider EK, Zhu Z (1998) Sensitivity of the Simulated Annual Cycle of Sea Surface Temperature in the Equatorial Pacific to Sunlight Penetration. J Climate 11:1932–1950

Shell KM, Frouin R, Nakamoto S, Somerville RCJ (2003) Atmospheric response to solar radiation absorbed by phytoplankton. J Geophys Res 108:4445. doi:10.1029/2003JD003440

Strutton PG, Chavez FP (2004) Biological heating in the equatorial Pacific: Observed variability and potential for real-time calculation. J Climate 17(5):1097–1109

Sweeney C, Gnanadesikan A, Griffies SM, Harrison MJ, Rosati AJ, Samuels BL (2005) Impacts of shortwave penetration depth on large-scale ocean circulation and heat transport. J Phys Oceanogr 35(6):1103–1119

Timmermann A, Jin FF (2002) Phytoplankton influences on tropical climate. Geophys Res Lett 29:2104. doi:10.1029/2002GL015434

Timmermann R, Goosse H, Madec G, Fichefet T, Ethe C, Dulière V (2005) On the representation of high latitude processes in the ORCA-LIM global coupled sea ice-ocean model. Ocean Model 8:175–201

Uppala SM et al (2005) The ERA-40 re-analysis. Q J R Meteorol Soc 131:2961–3012. doi:10.1256/qj.04.176

Valcke S, Caubel A, Vogelsang R, Declat D (2004) Oasis3 ocean atmosphere sea ice soil user's guide. Technical Report TR/CMGC/04/68, CERFACS, Toulouse, France

Vichi M, Masina S (2009) Skill assessment of the PELAGOS global ocean biogeochemistry model over the period 1980–2000. Biogeosciences 6:2333–2353

Vichi M, Masina S, Pinardi N (2007a) A generalized model of pelagic biogeochemistry for the global ocean ecosystem. Part I: Theory. J Mar Syst 64(1–4):89–109

Vichi M, Masina S, Navarra A (2007b) A generalized model of pelagic biogeochemistry for the global ocean ecosystem. Part II: Numerical simulations. J Mar Syst 64(14):110–134

Vichi M, Manzini E, Fogli PG, Alessandri A, Patara L, Scoccimarro E, Masina S, Navarra A (2011) Global and regional ocean carbon uptake and climate change: Sensitivity to an aggressive mitigation scenario. Clim Dyn 37:1929–1947. doi:10.1007/s00382-011-1079-0

Wetzel P, Maier-Reimer E, Botzet M, Jungclaus J, Keenlyside N, Latif M (2006) Effects of ocean biology on the penetrative radiation in a coupled climate model. J Climate 19(16):3973–3987